GE Research &
Development Center

A Theoretical and Experimental Evaluation of the Diffuse Reflectance from Rough Surfaces

S.Y. Hobbs, S.F. Feldman, H. Hatti, and J.T. Bendler

97CRD066, May 1997
Class 1

Technical Information Series

Corporate Research and Development

Technical Report Abstract Page

Title	A Theoretical and Experimental Evaluation of the Diffuse Reflectance from Rough Surfaces		
Author(s)	S.Y. Hobbs S.F. Feldman* H. Hatti* J.T. Bendler‡	**Phone**	(518)387-6394 8*833-6394
Component	Polymer and Inorganic Systems Laboratory		
Report Number	97CRD066	**Date**	May 1997
Number of Pages	17	**Class**	1
Key Words	reflectance, gloss, injection molding, surface, appearance		

A normalized theoretical expression describing the overall reflectance from a roughened surface was developed and tested against data obtained using a goniospectrophotometer. Samples were injection molded using textured molds having a range of roughness scales and then coated with 600 Å of aluminum. The surfaces were characterized by mechanical profilometry and relevant mathematical descriptors of the surface topographies were extracted by digital image analysis. The calculated and measured reflectance values agree well for incidence angles of 20° and 60° over a wide range of reflected intensities. At higher angles (82°), the measured reflectance values are more specular. Possible reasons for these discrepancies are discussed.

Manuscript received April 16, 1997

*Manufacturing Technology Laboratory
‡Dept. of Chemistry and Chemical Engineering, South Dakota School of Mines & Technology, Rapid City, SD 47701

A Theoretical and Experimental Evaluation of the Diffuse Reflectance from Rough Surfaces

S.Y. Hobbs, S.F. Feldman, H. Hatti, and J.T. Bendler

INTRODUCTION

During the last several years material suppliers, particularly those producing engineering thermoplastics, have become increasingly concerned with the visual appearance of molded parts. This concern has been driven by the need to build specific color and gloss characteristics into structural resins in order to reduce costs and emissions associated with secondary finishing. The problem is compounded by the fact that, in many applications, the initial appearance as well as the structural integrity of the material must be maintained over relatively long weathering periods.

The measurement of gloss and color is a well-developed science and numerous standards have been developed to quantify these attributes of appearance [1]. A primary deficiency of many of the methods is their failure to precisely relate specific structural or morphological characteristics of the substrate (e.g. its roughness) to the way in which light interacts with the material and thence to what is seen by the naked eye. These limitations have become more pronounced as techniques for very detailed characterization of surfaces, such as atomic force microscopy (AFM), have become generally available and digital image processing techniques have advanced to the point where precise numerical description of surface topography can be readily obtained. With these advances has come the desire to better predict the optical performance of parts as their surface and subsurface morphologies are altered by changes in composition, processing, or environmental exposure.

The relationship between "what we see" and "what we measure" is complex even for those cases in which geometric attributes rather than color dominate the appearance of the surface. This complexity results from the fact that the human eye and brain tend to associate various subjective qualities with different parts of the angular scattering 'window'. An example is shown in Figure 1 [2]. The diagram emphasizes the importance of being able to accurately predict the scattering characteristics of a particular surface as a first step in developing an analytical description of its visual appearance.

In this study an explicit expression describing the diffuse reflectance from conductive surfaces having known roughnesses and correlation lengths is developed. The expression is properly normalized so that the reflected intensity integrated over all observation angles is equal to the incident intensity. The accuracy of the theoretical expression is tested against goniospectrophotometer data obtained on samples having a range of well-characterized roughnessscales.

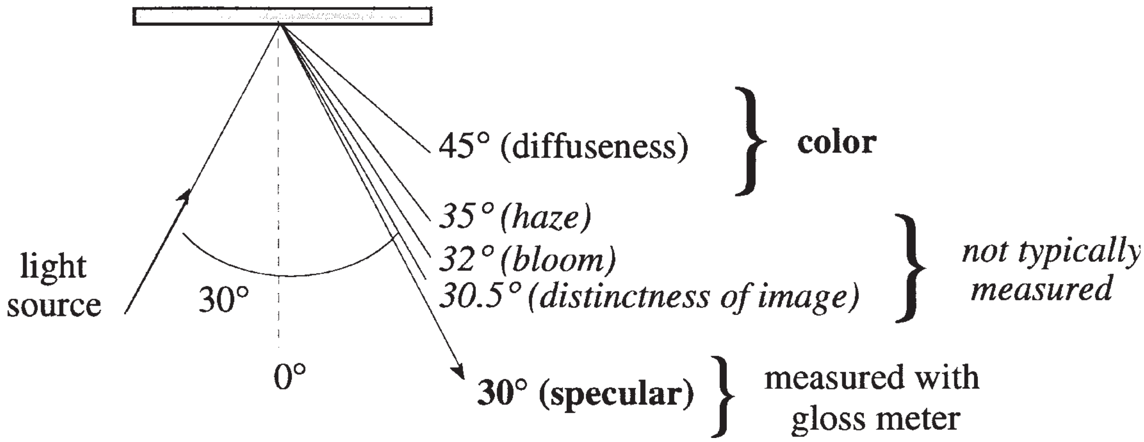

Figure 1: Schematic diagram showing the visual characteristics associated with light scattered at various angles [2].

EXPERIMENTAL

Sample Preparation and Description

The samples used in this study were injection molded from crystal polystyrene resin pigmented with low levels of carbon black. The mold surface was textured by Mold-Tech® and was divided into a number of separate areas having different microscopic surface roughness values. The textures were selected to provide a broad range of gloss levels and were sufficiently fine that the individual textural features remained invisible to the naked eye. Gloss values were measured at 20°, 60° and 85° according to ASTM procedure D523 using a BYK Gardner micro-TRI-gloss meter equipped with a black glass standard having a refractive index, $\eta = 1.567$. The texture designations and measured gloss values for the parts are listed in Table I.

Table I. Texture Designations* and Measured Gloss Values**

Texture	20° Gloss	60° Gloss	85° Gloss
MT11001	12	60	92
MT11003	7	36	70
MT11004	2	14	51
MT11006	1	6	12

* Mold-Tech texture identification number

** Measured according to ASTM D523

® Mold-Tech is a Division of Roehlin Inductries

Surface Roughness Measurements

Surface roughness measurements were made using a Tencor P-1 long scan profiler (Tencor Instruments Inc.) equipped with a diamond stylus having a 0.8 μm tip and a 70° shank angle. The tip force was 15 mg. For each sample, several 100 equally spaced line scans were run over a 1 mm^2 area. The data were digitized and used with an interpolation program to construct three dimensional surface profiles. These were displayed as 256 × 256 pixel images using hardware and software available on Parks Scientific atomic force microscope. Values for the root mean square roughness (σ) and root mean square slope ($m = \sqrt{2}\sigma / a$) were calculated for each scan and averaged for each of the four samples of interest.

Metallization

Since the express purpose of the current study was to develop an explicit relationship between diffuse reflectance and surface roughness in the absence of refraction and subsurface scattering and absorption, it was necessary to apply a conductive coating to the surfaces of the molded polystyrene plaques. This was accomplished by vacuum metallization of a thin film of aluminum. To minimize the film thickness and, at the same time, insure that the surface was optically opaque, a series of progressively thicker coatings were applied to clean glass slides and their reflectance characteristics were compared with those of a standard front surface mirror (obtained from Melles Griot). The results are plotted in Figure 2. A coating thickness of 600 Å was found to meet the desired criteria and samples with thicker coatings showed no difference in reflectance. Profilometer traces of the plaques before and after application of the coating showed that the roughness and slope values were unchanged within experimental error.

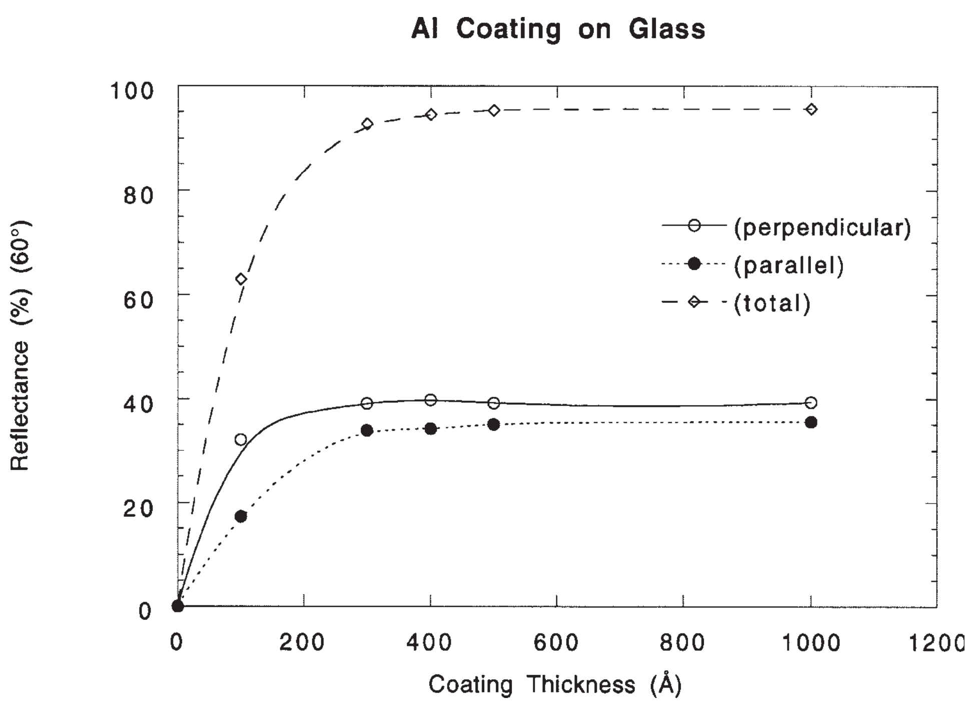

Figure 2: Plot showing variation in surface reflectance for aluminized glass surface as a function of coating thickness.

Reflectance Measurements

An Ocean Optics spectrometer with fiber optic probes and collection optics mounted on rotation stages as shown in Figure 3 was used to measure reflectance as a function of angle. A tungsten-halogen lamp illuminated the samples through the visible region. The light from the lamp is directed into a 400 μm diameter bifurcated fiber. One end of the fiber directs light to the sample (referred to as the illumination fiber) and the second is connected to the reference channel on the spectrometer. To control the size and cone angle of the illumination, light exiting the illumination fiber is first collimated by a 10 mm focal length lens (L1), passed through a 2 mm aperture and then re-collimated to a larger spot by a 100 mm focal length bi-convex lens (L2). An ellipsoidal illuminated area is determined by the angle of the illuminating beam relative to the sample. Reflected light is captured and collimated by a detection system consisting of a pair of 1000 mm focal length lenses (L3 and L4) separated by 72 mm followed by a 10 mm focal length lens (L5) which focuses light into the optical fiber. It is critical to ensure that all light is collected independent of the angular position of the detection assembly. The up-collimator assures that the sampled area is always larger than the illuminated ellipse. The sample is mounted in a holder allowing for five degrees of freedom (x, y, z, pitch, and yaw). Initially the illumination and detection arms are set to the same angle and the height and tilt of the sample relative to the fiber assemblies are adjusted to ensure that specularly reflected light is fully collected. Then the sample position is fixed and only the angle of the detection assembly is varied to measure diffuse reflectance. The incident light intensity is estimated by placing a mirror of known reflectance in place of the sample. Subsequent samples are compared to the mirror and absolute reflectances for each sample are obtained by correcting for the mirror reflectance.

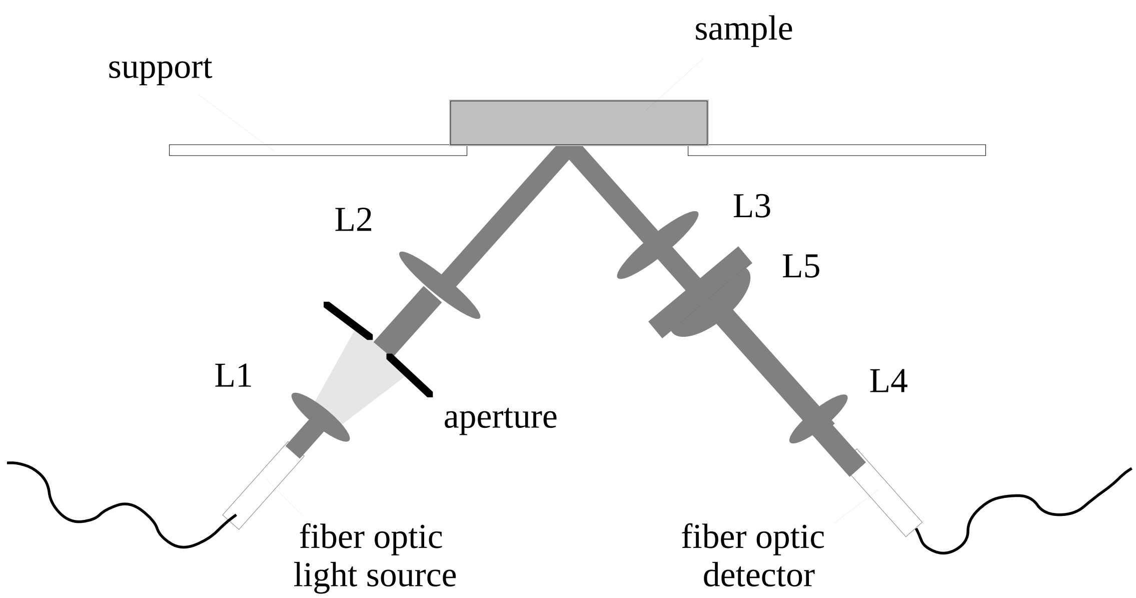

Figure 3: Schematic diagram of Ocean Optics goiniospectrophotometer.

The amount of light collected is critically dependent on the collection cone angle. The assumption was made that light emanates from (or is collected by) the optical system in a perfect linear cone. By measuring the diameter of a light beam at the sample holder and at a point 545 mm away an upper bound of 0.47 degrees was established for the collection cone half-angle.

THEORY

The scattering of electromagnetic radiation from rough surfaces has received considerable attention in the literature beginning with the pioneering work of Lord Raleigh at the turn of the century [3]. Many early studies focused on those cases where the irregularities were large compared to the illumination wavelength (*i.e.* the geometric optics region) and dealt primarily with regular surface arrays of asperities having well-defined geometries such as cones or half-cylinders [4,5].

The first generalized treatment of scattering from rough surfaces having a roughness scale smaller than the illumination wavelength was developed by Bennet and Porteus [6] based on a statistical treatment first proposed by Davis [7]. In their analysis, the specular reflectance at normal incidence is given as

$$R_{specular} = R_o \exp\left[-(4\pi\sigma / \lambda)^2\right] \tag{1}$$

where *Ro* is the reflectance from a corresponding smooth surface, σ is the root mean square roughness and λ is the wavelength of the incident radiation. The root mean square roughness is the standard deviation of the roughness measured from the mean surface height. The diffuse reflectance *at the specular angle* is given as

$$R_{diffuse} = R_o \frac{2^5\pi^4}{m^2}(\sigma / \lambda)^4(\Delta\phi)^2 \tag{2}$$

where ϕ is the acceptance angle of the detector and m is the root mean square slope. The latter is related to the correlation length through the expression

$$a = \sqrt{2}(\sigma / m) \tag{3}$$

Inspection of Equation 2 shows that the diffuse reflectance falls off very quickly at longer wavelengths (or lower roughness values). This behavior leads to the interesting although counterintuitive result, that the specular reflectance for small values of σ/λ is dependent only on the root mean square surface roughness and is independent of the slope.

It has been shown that Equation 1 can be extended to other incidence/reflection angles with relatively simple modification [8] to give

$$R_{specular} = R_o \exp\left[-(4\pi\sigma\cos\theta/\lambda)^2\right] \quad (4)$$

where θ is the angle of incidence. A similar expression for the specular reflectance was later derived by Beckmann and Spizzichino following a somewhat different approach [9].

Equation 4 is properly bounded giving a reflectance (R/R_o) value of 1 as the surface roughness drops to zero and approaching zero as the surface roughness becomes large compared with the incident wavelength. This is not true of the expression for $R_{diffuse}$ which quickly becomes very large as σ/λ rises.

The failure of Equation 2 has been attributed to the inability of the autocovarience function to represent the reflectance at large σ/λ values [10]. Following a slightly different development of the original theory, Porteus proposed an alternate expression for the diffuse term which circumvented some of the earlier difficulties. In this analysis

$$R_{diffuse} = R_o\left\{1-\exp\left[-(4\pi\sigma/\lambda)^2\right]\right\}\times\left\{1-\exp\left[-(\pi\alpha a/\lambda)^2\right]\right\} \quad (5)$$

where the rms slope is again defined by Equation 3 and the instrumental acceptance angle is given as $\pi\alpha^2$. In contrast to the expression in Equation 2, Equation 5 displays an acceptable upper bound of R_o for both large and small values of σ/λ. However, when the expression is re-written in terms of the rms slope, *m*,

$$R_{diffuse} = R_o\left\{1-\exp\left[-(4\pi\sigma/\lambda)^2\right]\right\}\times\left\{1-\exp\left[-(\sqrt{2}\sigma\alpha\pi/m\lambda)^2\right]\right\} \quad (6)$$

the overall reflectance is predicted to decrease with increasing slope in opposition to what is observed experimentally. This behavior, combined with difficulty extending the equation to the case of non-normal incidence, limits the utility of the Equation 5

Following the work of Bennett and Porteus, the problem of scattering from rough surfaces has been analyzed in great detail by many workers, and much of this prior work is conveniently summarized in the monograph by Beckman and Spizzichino [9]. It is therefore not necessary to review this early mathematical work for present purposes, other than to observe that the detailed expressions for diffuse scattering found in reference [9] are certainly not normalized in any obvious manner, and thus are not able in general to be conveniently tested by experiment. In addition, a number of misprints in key equations produce difficulties in following the analysis presented. Since our purpose is to use the results of scattering theory to interpret our experimental measurements, it is essential to have an analytical result which, when integrated over all scattering angles, produces a total scattering intensity equal to the original incident intensity on the surface (assuming no absorption has taken place). We now briefly summarize the basic analysis of scattering from rough surfaces as found in chapters 3-5 of Beckman and Spizzichino [9], with the important difference that we require at all times that the expressions for the scattering intensity exhibit proper normalization.

We begin with the Helmholtz-Kirchhoff integral theorem [9,11] for the scattered field E_2 (P) at an observation point P, a scalar distance R' from a point x,y, $\zeta(x,y)$ on the surface S;

$$E_2(P) = \frac{1}{4\pi}\iint_S \left(E\frac{\partial \psi}{\partial n} - \psi \frac{\partial E}{\partial n} \right) dS \tag{7}$$

where

$$\psi = \frac{e^{ik_2 R'}}{R'} \tag{8}$$

and **n** is the normal vector to the surface S at the point x,y, $\zeta(x,y)$. We use the conventions of reference 9, so that positions are specified in terms of Cartesian coordinates x,y,z with origin 0 and unit vectors $\mathbf{x_0},\mathbf{y_0},\mathbf{z_0}$. All quantities associated with the incident field are denoted by the subscript 1 and those associated with the scattered field have the subscript 2. The rough surface itself is given by the function

$$\zeta = \zeta(x,y) \tag{9}$$

and the mean height of the surface is the plane

$$z=0 \tag{10}$$

A major approximation of the theory is use of the Kirchhoff expressions for the field and its normal derivative at the surface, namely ;

$$(E)_S \approx (1+\tilde{R})E_1 \tag{11}$$

and

$$\left[\frac{\partial E}{\partial n}\right]_S = (1-\tilde{R})E_1 \mathbf{k_1} \bullet \mathbf{n} \tag{12}$$

where $\tilde{R}$ is the Fresnel reflection coefficient of a completely smooth surface and the propagation vector of the incident wave is

$$\mathbf{k_1} = \frac{2\pi}{\lambda}\frac{\mathbf{k_1}}{k_1} \tag{13}$$

with λ the wavelength of the radiation. Using the Kirchhoff approximations of Equations 11 and 12, Beckman and Spizzichino [9] show that the normalized scattering coefficient ρ from a perfectly conducting surface rough in two dimensions can be written

$$\rho = \frac{F_3}{A}\iint_A e^{i\mathbf{v}\cdot\mathbf{r}} dxdy \tag{14}$$

where

$$F_3(\theta_1,\theta_2,\theta_3)=\frac{1+\cos(\theta_1)\cos(\theta_2)-\sin(\theta_1)\sin(\theta_2)\cos(\theta_3)}{\cos(\theta_1)\left[(\cos(\theta_1)+\cos(\theta_2)\right]} \tag{15}$$

and

$$\mathbf{v}=k\left[(\sin\theta_1-\sin\theta_2\cos\theta_3)\mathbf{x_0}-\sin\theta_2\cos\theta_3\mathbf{y_0}-(\cos\theta_1+\cos\theta_2)\mathbf{z_0}\right] \tag{16}$$

with $k={}^{2\pi}\!/_{\lambda}$. In Equation 14 A is the area of S projected onto the xy plane. A misprint in the expression for F_3 on page 29 of reference 9 has been corrected in Equation 15 above. Equation 14 ignores edge effects and also assumes that the polarization of the incoming light is vertical [9]. The coefficient is given by the ratio of the intensity of the scattered field to the field scattered in the specular direction by a perfectly smooth, infinitely conducting surface, thus

$$\rho\equiv\frac{E_2}{E_{20}} \tag{17}$$

As a simple model of a rough surface, we now introduce a normally distributed rough surface as defined in [9]. That is, the surface height ζ is taken to have a normal distribution with mean value of zero (see Equation 10) and standard deviation s, so the distribution of the height fluctuations is given by

$$w(z)=\frac{1}{\sigma\sqrt{2\pi}}e^{-z^2/2\sigma^2} \tag{18}$$

We use the symbol $\langle\ \rangle$ to designate the mean value of a random variable, so that

$$\langle\zeta\rangle=\int_{-\infty}^{\infty}\zeta(x,y)w(\zeta(x,y))dxdy=0.$$

As a more complicated application of the averaging technique, consider the mean value of the integral

$$\left\langle\int_{-L}^{L}\int_{-L}^{L}e^{i\mathbf{v}\cdot\mathbf{r}}dxdy\right\rangle=\left\langle e^{iv_z\zeta}\right\rangle\int_{-L}^{L}\int_{-L}^{L}e^{iv_x x+iv_y x}dx=\chi(v_z)\rho_{0xy} \tag{19}$$

where $\chi(v_z)=\exp(-\frac{1}{2}\sigma^2v_z^2)$ is the characteristic function of the height fluctuations and

$$\rho_{0xy}=\frac{\sin(v_xL)}{v_xL}\frac{\sin(v_yL)}{v_yL} \tag{20}$$

is the scattering coefficient of a smooth conducting surface of area $A=4L^2$. The components v_x,v_y,v_z refer to the Cartesian components of **v** in Equation 16.

To complete the description of the rough surface model, we also need to specify the distance between the hills and valleys on the surface, that is, we need to know how far apart on average are the surface irregularities. We use the familiar Gaussian model for the roughness autocorrelation coefficient [9];

$$C(r_1, r_2) = \frac{\langle \zeta(r_1)\zeta(r_2) \rangle}{\langle \zeta^2(r_1) \rangle} = e^{-(r_1 - r_2)^2 / a^2} \tag{21}$$

where a is the correlation length of the corrugations. The total energy scattered into a given direction is proportional to $\rho\rho^*$ and the mean energy scattered into a given direction is proportional to $\langle \rho\rho^* \rangle$. Using Equations 17 to 21 above, and following the methods of reference 9, we eventually find that the average energy scattered into a given direction is given by

$$Energy \propto e^{-g}\left[\rho_{0xy}^2 + \pi \frac{F_3^2 a^2}{\lambda^2} \sum_{m=1}^{\infty} \frac{g^m}{m m!} e^{-(v_x^2 + v_y^2) a^2 / 4m} \right] \tag{22}$$

where we have introduced the symbol from reference 9

$$g = \frac{4\pi^2 \sigma^2}{\lambda^2} \left[\cos\theta_1 + \cos\theta_2 \right]^2 \tag{23}$$

Following Born and Wolf [11], it is convenient for the purpose of normalization to introduce Cartesian p,q components of the scattering cone;

$$v_x^2 = k^2 \left[(\sin\theta_1 - \sin\theta_2 \cos\theta_3)^2 \right] = k^2 p^2 \tag{24}$$

$$v_y^2 = k^2 \left[\sin\theta_2 \cos\theta_3 \right]^2 = k^2 q^2 \tag{25}$$

The reflectance ratio $\Re$ will be defined as the fraction of energy scattered in a given direction compared to the energy that would be scattered by a smooth conducting surface in the specular direction. Introducing p and q from Equations 24 and 25 into Equation 22 gives

$$\Re = e^{-g}\left[\delta(p)\delta(q) + \pi \frac{F_3^2 a^2}{\lambda^2} \sum_{m=1}^{\infty} \frac{g^m}{m m!} e^{-(p^2 + q^2) k^2 a^2 / 4m} \right] \tag{26}$$

where δ are Dirac delta functions specifying that the first term <u>only</u> contributes in the specular direction. Now integrating Equation 26 over all possible p and q , extending the ranges to plus and minus infinity with no significant loss of accuracy, gives

$$\int_{-\infty}^{\infty} \int_{-\infty}^{\infty} \Re \, dp\, dq = e^{-g} \left[1 + e^{g} - 1 \right] = 1 \tag{27}$$

showing that Equation 26 is properly normalized. When Equation 26 is utilized in connection with an experimental detector which allows scattered light to be received within a cone of angular extent ε, then Equation 26 must be integrated over the range p,q from $-\varepsilon$ to ε for each observation direction.

For rough surfaces and non-grazing angles of incidence, the relevant values of g in Equation 26 are g >5 or so, and the delta function terms in Equation 26 may be safely ignored. Also, if the acceptance angle ε of the detector is not too large, then the variation of the intensity across the detector opening at any given angle will be small, and the large g limit of Equation 26 may be used;

$$\Re = 4\pi\varepsilon^2\left[\frac{1+\cos(\theta_1+\theta_2)}{\cos(\theta_1)(\cos\theta_1+\cos\theta_2)}\right]^2\left[\frac{a^2}{\lambda^2 g}\right]\exp\left[\frac{-V_{xy}{}^2a^2}{4g}\right] \tag{28}$$

where

$$g = \frac{4\pi^2\sigma^2}{\lambda^2}\left[\cos\theta_1+\cos\theta_2\right]^2 \tag{29}$$

and

$$V_{xy}{}^2 = \frac{4\pi^2}{\lambda^2}\left[\sin\theta_1-\sin\theta_2\right]^2 \tag{30}$$

and θ_1 is the incident angle (from the surface normal), θ_2 is the scattering direction, ε is the solid angle of the detector opening, and a is the spatial correlation length of the irregularities. Expression (28) has been used to fit to all of the scattering data in the present study.

For small surface roughness, the delta functions in Equation 26 cannot be ignored and the variation of the intensity across the detector opening can be considerable. In this case, if the relevant values of g are g < 1, and the small g limit of Equation 26 results in

$$\Re = \Re_1 + \Re_2 \tag{31}$$

where

$$\Re_1 = e^{-g}\left[H(p_0-\varepsilon)-H(p_0+\varepsilon)\right]\left[H(q_0-\varepsilon)-H(q_0+\varepsilon)\right] \tag{32}$$

and

$$\Re_2 = e^{-g}\left\{\pi\frac{F_3^2a^2}{\lambda^2}\left(\frac{\pi}{\beta}\right)\sum_{m=1}^{\infty}\frac{g^m}{m!}erf(\left\{\varepsilon\sqrt{\frac{\beta}{m}}\right\}\left[erf((p_0+\varepsilon)\sqrt{\frac{\beta}{m}})-erf((p_0-\varepsilon)\sqrt{\frac{\beta}{m}})\right]\right\} \tag{33}$$

where H's are the Heaviside step functions, erf is the error function and

$p_0 = \sin\theta_1 - \sin\theta_2,\ q_0 = \sin\theta_2$, and $\beta = \frac{a^2\pi^2}{\lambda^2}$. In a later study we will examine the ability of Equation 33 to represent scattering from smooth surfaces.

RESULTS

Digital images of the individual sample surfaces are presented in Figure 4(a)- 4(d) and their respective roughness and slope values are listed in Table II. The vertical scales have been adjusted to accentuate the individual topographical features of each surface. A better comparison of the roughness variations among the four samples is provided in Figure 5 where the cumulative height distributions have been shifted to the same mean value and overlaid. It should be remarked that the surface profiles for each sample were remarkably reproducible. This feature is illustrated in Figure 6 where the height distributions taken from five different $1mm^2$ areas of sample 11003 are seen to be almost coincident. The corresponding σ and m values shown in Table III are likewise very similar.

The measured and calculated reflectance values for the four surfaces are plotted in Figures 7(a) - 7(d) and 8(a) - 8(d). The incident angles were selected to correspond as closely as possible with the suggested ASTM angles used to characterize surface gloss (typically 20°, 60°, and 85°*). Note the large differences in the vertical scales among the various graphs. The agreement between the observed and calculated reflectance values is quite good for the 20° and 60° reflectance angles in spite of the fact that the reflected intensities vary over approximately two orders of magnitude.

Larger differences between the observed and calculated reflectance levels are observed for the 82° plots. In each case the data indicate that the surface reflection is considerably more specular than predicted. The reasons for these discrepancies are not fully understood but part of the problem may be associated with the fact that the magnitude and width of the scattering envelope become highly angular dependent on approaching the grazing angle. An example is shown in Figure 9 for the case of surface 11004. Here the experimental data is plotted against the reflectance curves calculated for 82° and 85° incidence angles. The results show that variations of one or two degrees in the incidence angle can have a significant effect on the measured reflectance.

A second factor that may contribute to the differences in the observed and calculated values stems from the fact that the theoretical development assumes a Gaussian distribution of roughness. The extent to which this condition is satisfied experimentally may be evaluated by constructing probability plots of the roughness distributions. This is done in Figure 10(a) - 10d) for the surfaces analyzed in this study. None display most probable height distributions and at least one (11001) shows evidence of having multiple roughness scales. The extent to which these variations may affect the scattering results requires further investigation.

---

* Because of geometrical restrictions in the available instrumentation, the highest incident angle was restricted to 82° rather than 85°.

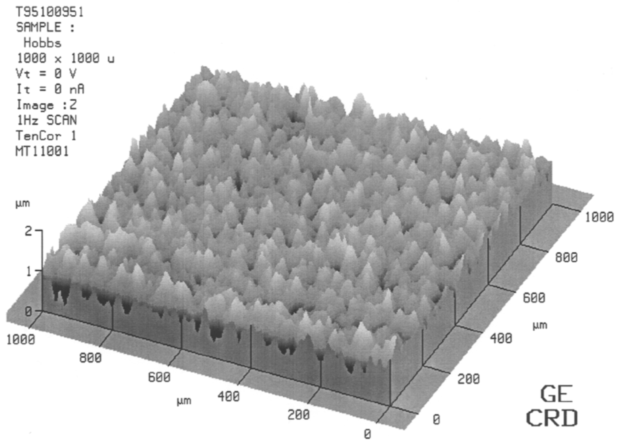

(a)

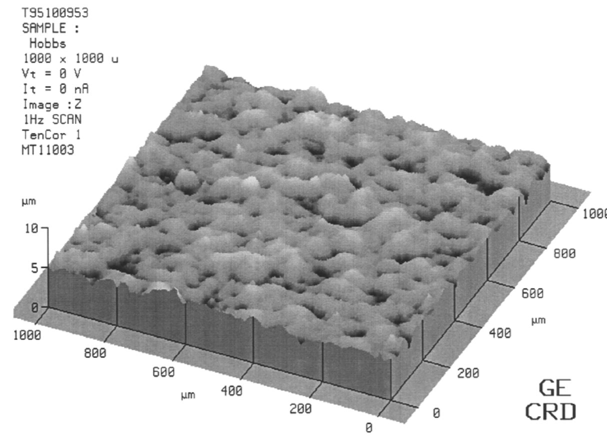

(b)

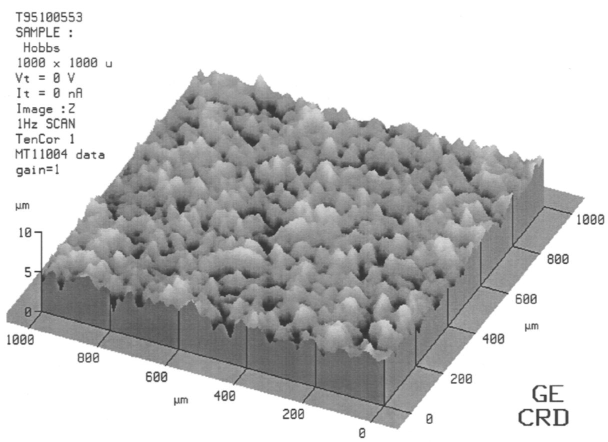

(c)

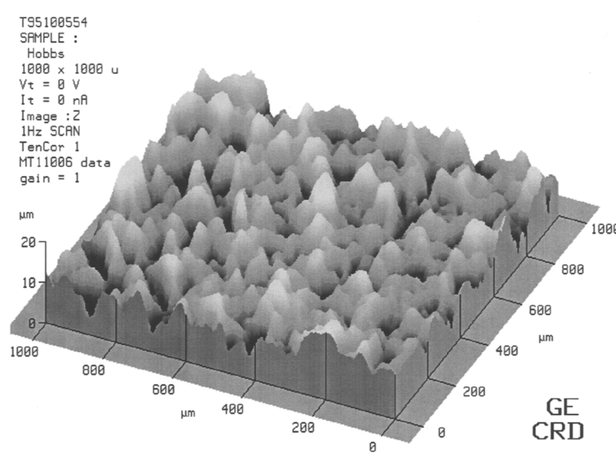

(d)

Figure 4: 3-D profilometer images of molded plaque surfaces (a) MT11001, (b) MT11003, (c) MT11004, (d) MT11006.

Table II. Surface Roughness Parameters

Texture	σ_{rms} (µm)	m_{rms}
MT11001	0.19	0.025
MT11003	0.46	0.04
MT11004	0.6	0.06
MT11006	2.5	0.19

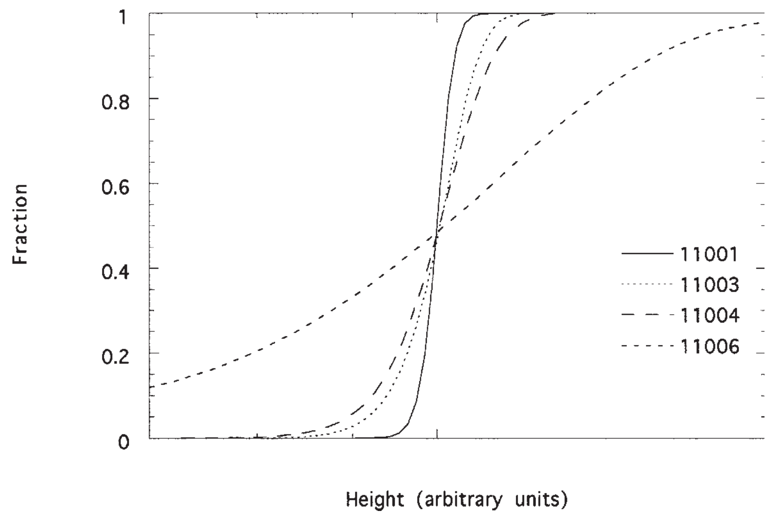

Figure 5: Comparison of cumulative height distributions for textured surfaces 11001, 11003, 11004 and 11006. The results have been shifted to the same mean value and overlaid to illustrate the progressive increase in the breadth of the height distributions (i.e. the rms height) as the surface roughness increases.

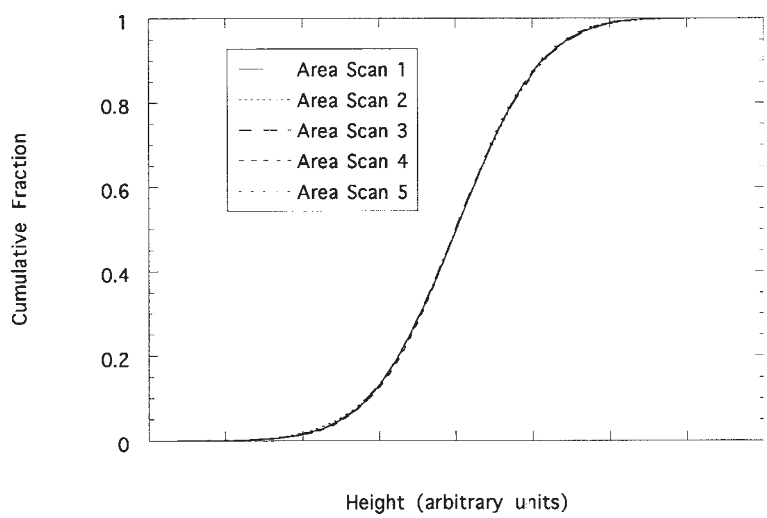

Figure 6: Overlay of the cumulative heights distributions taken from six different areas of sample 11003. The close agreement illustrates that excellent roughness uniformity is retained over the sample surface.

Table III. Surface Roughness Reproducibility

Texture	σ_{rms} (μm)	m_{rms}
11003 (area #1)	0.45	0.047
11003 (area #2)	0.46	0.046
11003 (area #3)	0.45	0.046
11003 (area #4)	0.44	0.045
11003 (area #5)	0.44	0.045

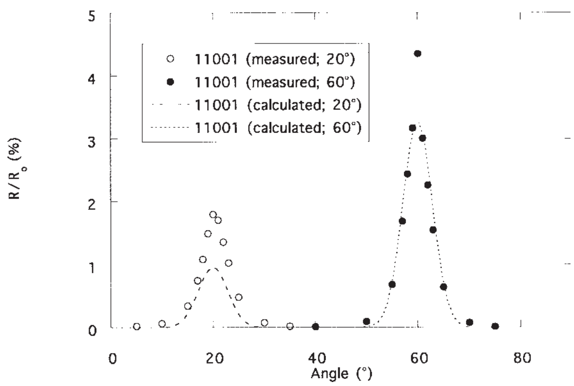

(a)

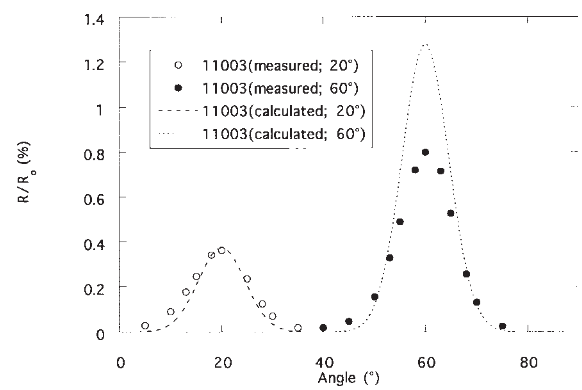

(b)

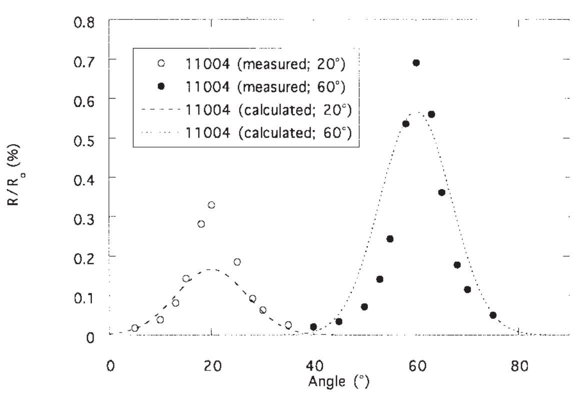

(c)

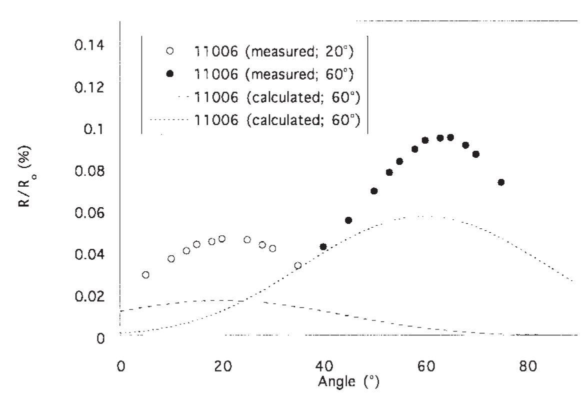

(d)

Figure 7: Measured and calculated reflectance curves (20° and 60° incidence) for surfaces (a)11001, (b) 11003, (c)11004, and (d)11006.

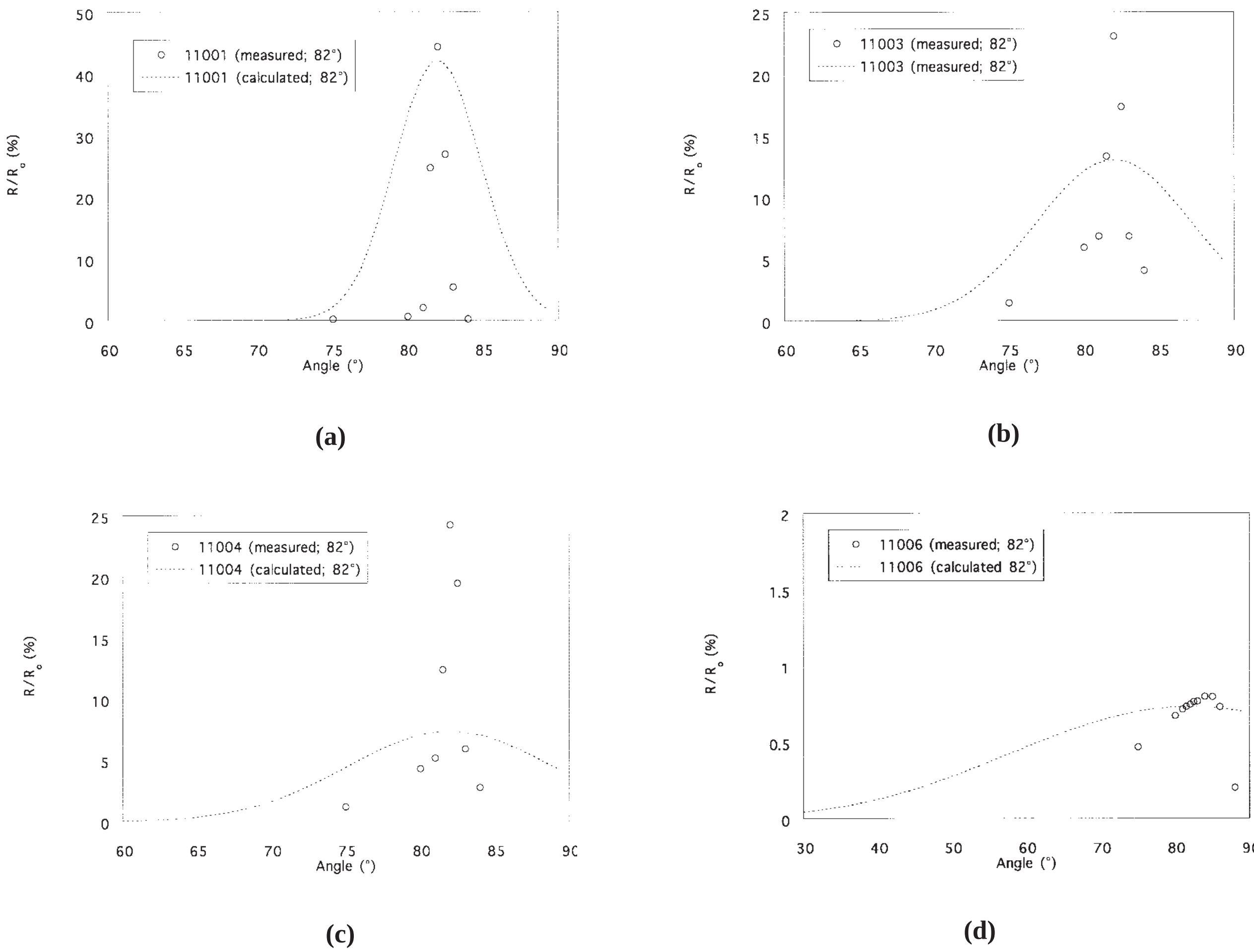

Figure 8: Measured and calculated reflectance curves (82° incidence) for surfaces (a)11001, (b)11003, (c)11004, and (d)11006.

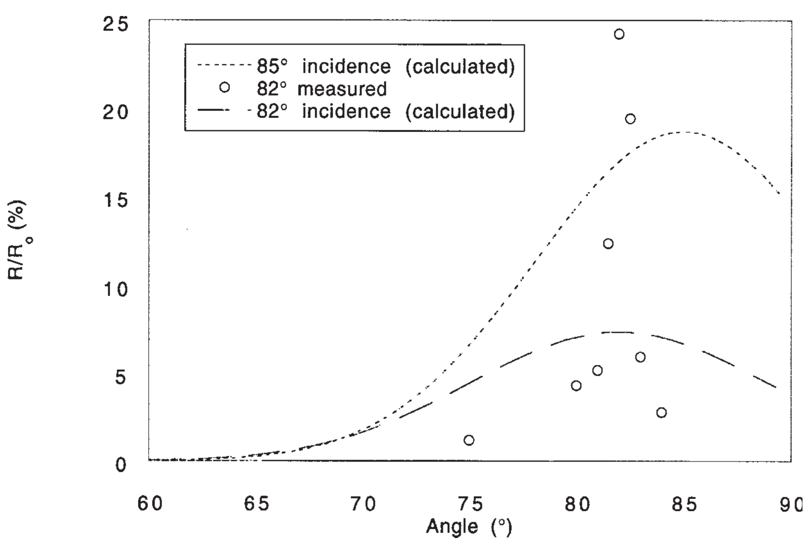

Figure 9: Comparison of 82° and 85° reflectance curves vs. measured values for surface 11004.

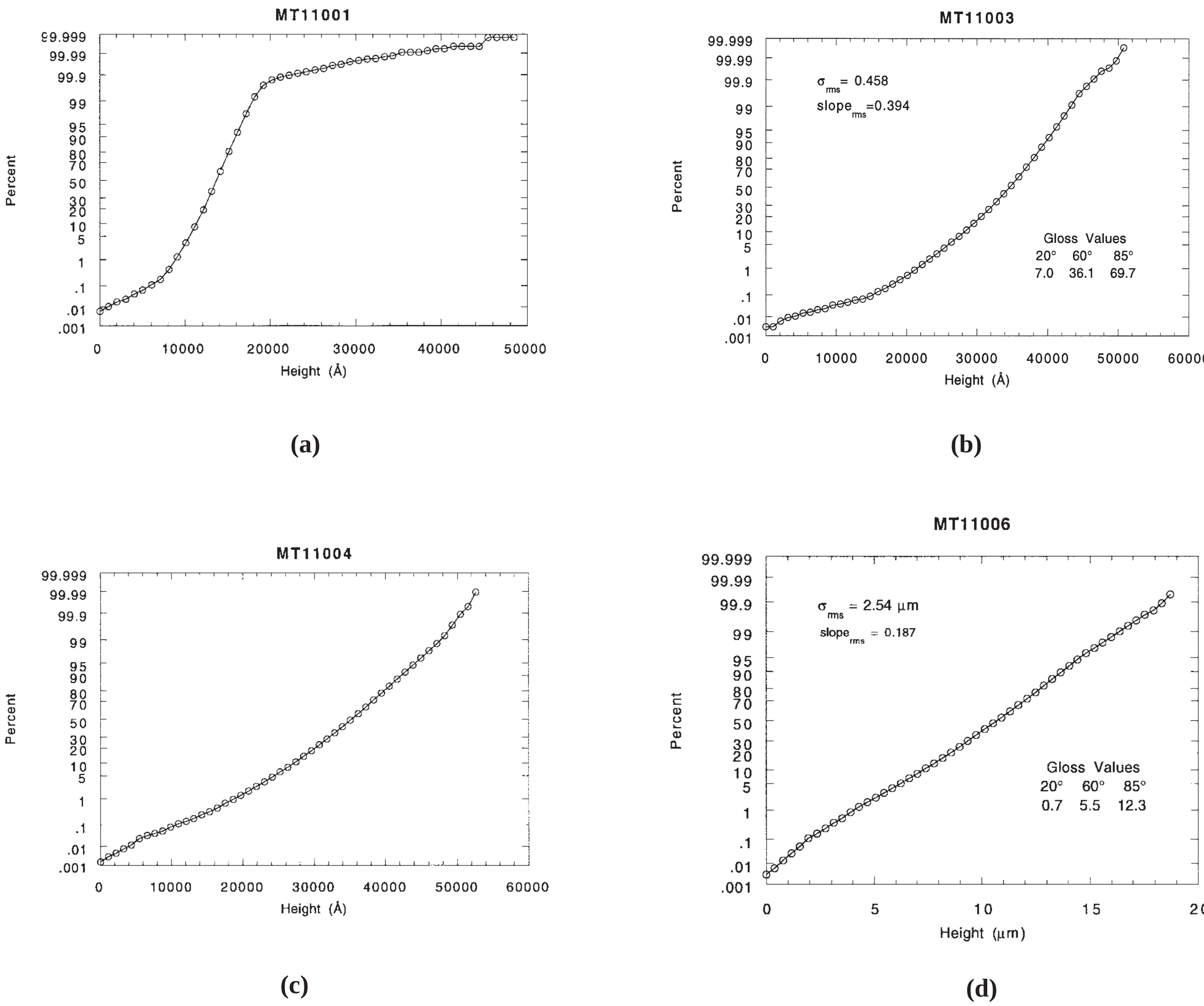

Figure 10: Probability plots of height distributions for surfaces (a)11001, (b)11003, (c)11004, and (d)11006. Straight lines indicate that the height distributions are Gaussian.

CONCLUSIONS

A new theoretical treatment of the reflectance from rough surfaces has been developed. In contrast to earlier derivations the results are properly normalized so that the reflected intensity is equal to the incident intensity when integrated over all scattering angles. The expression explicitly defines the relationship between the scattered light intensity and readily measured experimental parameters such as the surface roughness and slope and the detector acceptance angle. Reflectance values calculated from the new expression have been compared with values measured over a wide range of incident angles on surfaces having large differences in surface roughness. At low and intermediate incidence angles the agreement between theoretical and measured values is very good. At higher angles, the theoretical expression underestimates the specularity of the reflectance. The high sensitivity of the calculated values to small changes in incidence angle and the non-Gaussian character of the surface roughness of the available samples are believed to be partially responsible for the discrepancies.

ACKNOWLEDGMENT

The authors are indebted to Dr. W.G. Morris and Ms. Noel L. Jones for making the surface roughness measurements presented in this study.

REFERENCES

[1] ASTM Standards on Color and Appearance Measurement (5th Edition), ASTM, 100 Barr Harbor Drive, West Conschohocken, PA 19428-2529

[2] R.S. Hunter and R.W. Harold, “The Measurement of Appearance” (2nd ed.), Wiley-Interscience, John Wiley & Sons, New York (1987).

[3] Lord Raleigh, Phil. Mag. 14, 350 (1907).

[4] V. Tweedy, J. Appl. Phys. 22, 825 (1951); 24, 659 (1953).

[5] M. A. Biot, J. Appl. Phys. 28, 1445 (1957); 29, 998 (1951).

[6] H.E. Bennett and J.O. Porteus, J. Optical Soc. Am., 51,2 123 (1961).

[7] H. Davies, Inst. Elec. Engrs. (London) 101,209 (1954).

[8] A. S. Toporets, Opt. Spectroscopy 16, 54 (1964).

[9] P. Beckmann and A. Spizzichino, The Scattering of Electromagnetic Waves from Rough Surfaces, (Artech House, Inc., Norwood, MA (1987) (Originally published by Pergamon Press (1963).

[10] J.O. Porteus, J. Optical Soc. Am. 53, 12, 1394 (1963).

[11] M. Born and E. Wolf, Principles of Optics (Pergamon Press, Inc. New York, 1959), Sec. 8.3.3.

S.Y. Hobbs
S.F. Feldman
H. Hatti
J.T. Bendler

A Theoretical and Experimental Evaluation of the Diffuse Reflectance from Rough Surfaces

97CRD066
May 1997